An experimental and theoretical investigation of flow in a gross pollutant trap

J. T. Madhani[*], N. A. Kelson[**] and R. J. Brown[*]
[*]School of Engineering Systems, Queensland University of Technology, Garden Point Campus, Brisbane 4001, Australia, (Email: j.madhani@qut.edu.au; richard.brown@qut.edu.au)
[**]HPC & Research Support Group, Queensland University of Technology, Garden Point Campus, Brisbane 4001, Australia, (Email: n.kelson@qut.edu.au)

Abstract Flow through a gross pollutant trap (GPT) with fully blocked screens is investigated experimentally and theoretically using computational fluid dynamics (CFD). Due to the wide range of possible flow regimes, an experimental approach is developed which uses a downstream weir arrangement to control the nature of the flow and the variation in free surface height. To determine the overall flow structure, measurements are taken at a fixed depth throughout the trap with an Acoustic Doppler Velocimeter (ADV), including velocity profile data across three cross sections of the GPT suitable for more detailed comparison with simulations. Observations of the near-wall flow features at the free surface are also taken, due to their likely importance for understanding litter capture and retention in the GPT. Complementary CFD modelling (using Fluent 6.3) is performed using a two-dimensional k-ε turbulence model along with either standard wall law boundary conditions or enhanced near-wall modelling approaches. Comparison with experiments suggest that neither CFD modelling approach could be considered as clearly superior to the other, despite the significant difference in near-wall mesh refinement and modelling that is involved. The experimental approach taken here is found useful to control the flow regime in the GPT and further experiments are recommended to study a greater range of flow conditions.

Keywords Gross pollutant trap, GPT, CFD, Fluent.

INTRODUCTION

Stormwater is surface water runoff from urban areas discharging into receiving waterways. Pollutants in stormwater are collected on the urban runoff path and consequentially this can have a devastating effect on the environment and its natural habitants. This has led to the development of stormwater quality improvement devices (SQID) to efficiently trap urban waste of varying sizes such as sludge, silt, sediments and solids. Gross pollutant traps (GPTs) are a class of SQIDs that separate pollutants dimensionally greater than 5 mm (Allison, 1998) from stormwater. A GPT LitterBank shown in Fig. 1 was recently developed by C-M Concrete Pty Ltd, and it uses retaining screens (Fig. 2) to collect gross pollutants prior to the release of stormwater into natural waterways. Currently there are approximately 20 LitterBanks operating at strategic stormwater locations throughout Queensland, Australia.

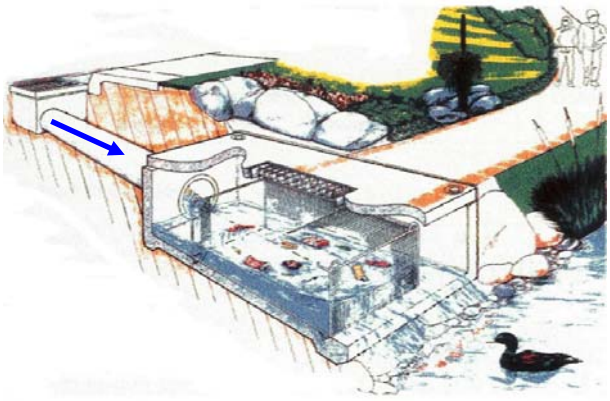

Fig. 1. GPT – LitterBank *in situ.*

Field monitoring of GPTs in Brisbane, Queensland indicates that during wet weather a wide range of inlet, outflow and other operating conditions are encountered. For example, the extent and duration of rainfall will influence the flow rate entering the trap. The tidal or flood levels of the downstream receiving waterways will determine the outflow level in the GPT. Due to infrequent cleaning, the retaining screens are often found to be blocked with organic matter. Partially or fully blocked screens can radically change the litter retention characteristics and flow structure within the GPT leading, for example, to large recirculating flow patterns within the trap area accompanied by

hydraulic short circuiting (Thackston et al., 1987) where the preferred outflow path is via the bypass channel (see Fig. 2).

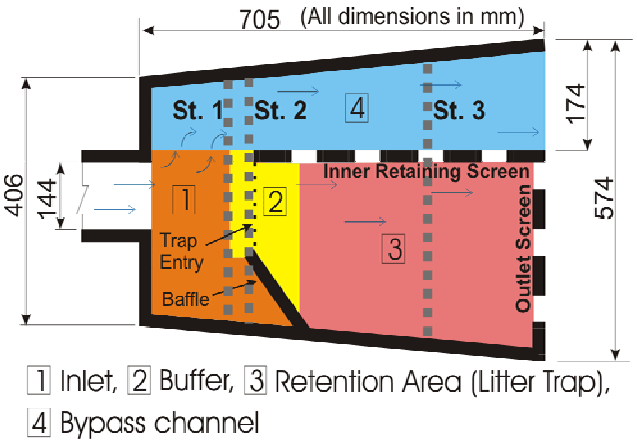

Fig. 2. Plan view of the LitterBank with the measurement stations St.1 (x = 137.5), St.2 (x = 182.5) and St.3 (x = 450).

Depending on the operating conditions, the possible flow regimes inside the GPT can range from turbulent time dependent free surface flows to more steady state conditions, and this presents significant challenges for either experimental or numerical studies aimed at understanding the flow and litter retention characteristics of the trap. To facilitate the study of steady state flow conditions, an experimental approach is developed here using a downstream weir arrangement to control the nature of the flow and the variation in free surface height in the GPT. The weir height can also approximate the elevated outflow water levels into the receiving waterway due to rainfall or storm events. An experimental rig of a scale model GPT with solid internal walls is used to study pollutant-free flow in a trap with fully blocked screens, and Acoustic Doppler Velocimeter (ADV) fluid point velocity data is collected at a fixed depth, mainly in the retention area and trap entry. Data is collected in more detail across three cross sections of the GPT (See Fig. 2) for comparison with simulations. Observations of the near-wall flow features at the free surface inside the GPT are also taken, due to their likely importance for understanding litter capture and retention. Further details of the experimental approach are provided later.

Supplementary to the experiments, simulations are performed to determine the suitability of CFD as a predictive tool for the case of an assumed steady state flow regime with a quiescent flat free surface. While acknowledging that the flow in the rig is likely to be three-dimensional, a simplified two-dimensional approach is taken in the simulations (using Fluent 6.3) using a k-ε turbulence model with standard and near-wall modelling functions. The simplifications used here avoid the prohibitive computational cost and modelling uncertainties involved in a fully three-dimensional approach, and also permit an investigation of the benefits or otherwise of increased numerical resolution for the prediction of the experimentally observed near-wall flow features at the surface. Details of the modelling are given below.

Regarding earlier research, to the Authors' knowledge work relating to ADV measurements or CFD on GPTs similar in design to the one studied has not been published. However, some work in the physical modelling of GPT designs with either real or simulated pollutants exists (Armitage and Rosseboom, 1999; Phillips, 1999). Hydrodynamic details of vector velocity field were not investigated. Combined ADV and CFD studies have been used to understand the hydrodynamic behaviour of fluids in vortex separators, dissolved air flotation (DAF) tanks, sedimentation basins and aquaculture raceways (Tyack & Fenner, 1999; Lundh et al., 2001; Ta et al., 2001; Huggins et al., 2003; Kwon et al., 2006; Park et al., 2006). Also, CFD studies with GPT related devices, such as sewage structures, storage/retention tanks and hydrodynamic separators have provided valuable insights into flow patterns, pollutant mixing and sediment transport behaviour (Stovin et al., 1999, 2000, 2002; Harwood, 2002; Faram and Harwood, 2003). Two-dimensional CFD models have been used to study global flow structures and sediment retention in invert traps (Buxton et al., 2002; Gupta et al., 2005).

EXPERIMENTAL METHOD

The experimental rig (50% scale model) was placed in a square section (19 m, 0.6 m width, 0.6 m depth) tilting flume at the QUT hydraulic laboratory. The flume inclination was set to horizontal and a constant flow rate was established via controller settings on the centrifugal pumps which circulate the water from underground storage tanks into the flume. Flow rate readings were checked with periodical measurements in the collection tank at the flume outlet. Flow into the GPT was through a horizontal partially filled 1.8 m section inlet pipe with internal diameter 144 mm. To promote smooth upstream flow conditions, three mesh screens 1 m apart were inserted at the upstream end of the flume. The height of the weir at the downstream end of the flume (not illustrated) was fixed at 92 mm above GPT floor.

Measurements were obtained for a flow rate through the GPT of 1.0 L/s, although some slow variations in the flow conditions (± 0.1 L/s) during the course of the experiments were unavoidable as a constant head tank was not fitted to the flume. The flow conditions in the flume were allowed to operate for a minimum of one hour prior to taking measurements, after which the water free surface in the GPT and also downstream was observed to be smooth and free of any obvious wave-like disturbances. Water free surface heights inside the trap and a further 2 m downstream were periodically measured relative to the GPT floor using vernier height gauges (resolution 0.1 mm). The upstream and downstream height measurements were found to be 94 mm ± 1 mm.

Regarding flow data acquisition in the scaled GPT, single point velocity measurements were taken using a Sontek™ UW ADV (10 MHz, serial No. 0510) signal condition module that is joined to a 50 mm downward-facing rigid stem probe (serial No. 0007). The ADV probe (Fig. 3) uses an acoustic remote sampling volume (using a transmitter and three receivers with 120º separation) based on the Doppler shift to measure the flow component velocities of the seeding particles in the water (Kraus et al., 1994; Lohrman et al., 1994; Voulgaris and Trowbridge, 1998; McLelland and Nicholas, 2000). The sampling volume is located 50 mm from the probe end (see A in Fig. 3) and diluted French chalk was used as seeding particles to improve the signal to noise ratios (SNRs). Apart from velocities, the ADV system also records the SNRs and the correlations (CORs) to filter signals that do not meet certain threshold values. The SNR and COR values indicate the quality of the data sampled. Measurements were taken at or above the Sontek recommended levels of 70% for the minimum COR and 15 dB for the minimum SNR to reduce measurement uncertainties. All measurements were sampled at 25 Hz for the duration of 180 s (time series length of 4500). For batch post processing ADV generated output data files, WinADV version 2.024 was used (Wahl, 2006).

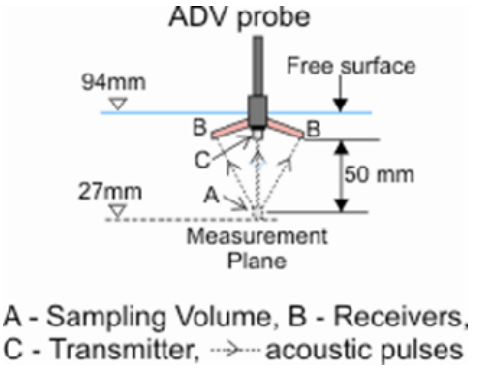

Fig. 3. Front view of upstream inlet structure showing the measured plane.

Due to the internal geometrical configuration of the GPT and the ADV probe, some difficulties were encountered in taking measurements close to the vertical side walls inside the trap, and obtaining data for near-wall distances less than 40 mm was not feasible. Flow data inside the GPT was measured at a fixed depth where the position of the ADV sampling volume was 27 mm from the GPT bed. Although desirable, ADV flow data acquisition closer to the free surface was not possible as the three acoustic receivers and the transmitter on the probe must be submerged for proper operation (SonTek, 2006). This requirement corresponds to a minimum submerged water depth of at least 60 mm for the ADV sampling volume.

Surface flow structures within the GPT were also observed using neutral buoyant particle seeding (20-50 μm). These were introduced onto the upstream free surface via a feeding system, or sprinkled directly onto the free surface in the retention area and the bypass channel. Repeated observations of the particles on the free surface were made, and estimates of the lengths of the flow features (estimated error ± 5 mm) recorded, included the zones close to the GPT walls.

COMPUTATIONAL FLUID DYNAMIC (CFD) STUDY

The modelling approach taken here assumes a steady state turbulent flow regime with a quiescent free surface of constant fixed height h throughout the computational domain. A 2D k-ε turbulence model (using Fluent 6.3) with either standard or near-wall modelling functions was used to compute the mean surface flow field $u_i(x,y)$, $(i = 1,2)$and variation with depth was accounted for via , $u_i(x,y,z) = u_i(x,y) \times s(z)$, where $s(z) = \left(\frac{z}{h}\right)^{\frac{1}{7}}$ is used. The present approach can be thought of as a simplification of the widely used depth-averaged k-ε model due to Rastogi & Rodi (1978). For a constant height free surface flow where horizontal shear is much larger than vertical shear, the vertical production terms are negligible compared to the horizontal production, and the Rastogi & Rodi model reduces to the standard 2D k-e model used here (Cea et al, 2007).

While acknowledging that the flow in the rig is likely to be three-dimensional, the simplifications used here permit a computationally feasible investigation of the benefits or otherwise of increased numerical resolution when using enhanced wall modelling (as described below) for the prediction of the experimentally observed near-wall flow features.

Turbulence modelling

To model the turbulence, Cartesian x and y axes were defined along and perpendicular to the primary flow direction in the GPT scale model, and the Reynolds Averaged Navier Stokes (RANS) equations were used to describe the steady incompressible mean flow quantities. The standard two-equation k-ε (denoted SKE) turbulence model was used, where the turbulent viscosity, μ_t the turbulent kinetic energy, k and dissipation rate, ε are described by the equations:

$$\frac{\partial}{\partial x_i}(\rho k u_i) = \frac{\partial}{\partial x_j}\left[\left(\mu + \frac{\mu_t}{\sigma_k}\right)\frac{\partial k}{\partial x_j}\right] + G_k - \rho\varepsilon \tag{1}$$

$$\frac{\partial}{\partial x_i}(\rho \varepsilon u_i) = \frac{\partial}{\partial x_i}\left[\left(\mu_t + \frac{\mu_t}{\sigma_\varepsilon}\right)\frac{\partial \varepsilon}{\partial x_j}\right] + C_{1\varepsilon}\frac{\varepsilon}{k}G_k - C_{2\varepsilon}\frac{\varepsilon^2}{k} \tag{2}$$

In equations (1) and (2) $G_k = \mu_t S^2$ is the turbulent production term, $S \equiv \sqrt{2S_{ij}S_{ij}}$ is the modulus of the mean rate of strain tensor $S_{ij} = \frac{1}{2}\left(\frac{\partial u_i}{\partial x_j} + \frac{\partial u_j}{\partial x_i}\right)$, the turbulent viscosity $\mu_t = C_\mu \frac{k^2}{\varepsilon}$ and the constant values are: $C_\mu = 0.09$, $\sigma_k = 1.0$, $\sigma_\varepsilon = 1.3$, $C_{1\varepsilon} = 1.44$, and $C_{2\varepsilon} = 1.92$.

Regarding the boundary conditions for the SKE model, standard logarithmic wall functions were used, where the near-wall mean velocity is evaluated via:

$$U^+ = \frac{1}{\kappa}\ln(Ey^+) \tag{3}$$

where U^+ and y^+ represent a dimensionless velocity and near-wall distance, and the values of κ and E are set to 0.42 and 9.8 respectively. The above logarithmic wall law is applied at the near-wall cells provided $y^+ \geq 11.225$ (For lower values of y^+ a linear relationship $U^+ = y^+$ is applied).

The influence of near wall modelling in the 2D flow field prediction was also investigated by using an SKE model with enhanced wall treatment (EWT). The EWT is intended to be used with near-wall mesh refinement and features a two layer method where a Reynolds number Re_y based on the near-wall distance is used to divide the flow domain into two regions. In the flow region $\mathrm{Re}_y \geq 200$ the SKE turbulence model is employed, while for $\mathrm{Re}_y < 200$ the one-equation Wolfshtein turbulence model is used (Wolfshtein, 1969). In the latter model, the k transport equation is retained, while ε and μ_t are expressed as algebraic functions of k and y only (y denoting here the normal distance to the nearest wall):

$$\varepsilon = \frac{k^{3/2}}{L\left[1-\exp\left(-\mathrm{Re}_y / A_\varepsilon\right)\right]} \quad \text{and} \quad \mu_t = C_\mu \rho \sqrt{k} L\left[1-\exp\left(-\mathrm{Re}_y / A_\varepsilon\right)\right] \tag{4}$$

where $L = \kappa C_\mu^{-3/4} y$, $Re_y \equiv \frac{\rho\sqrt{k}\,y}{\mu}$, $A_\mu = 70$, $A_\varepsilon = 2\kappa C_\mu^{-3/4}$ and $\kappa = 0.41$. The turbulent viscosity for the EWT model is computed (Jongen, 1992) by blending the viscosities μ_t obtained from the Wolfshtein (W) and the SKE models via:

$$\mu_{t,EWT} = \lambda_\varepsilon \left(\mu_t\right)_{\mathrm{SKE}} + \left(1-\lambda_\varepsilon\right)\left(\mu_t\right)_W \tag{5}$$

$$\text{where } \lambda_\varepsilon = \frac{1}{2}\left[1+\tanh\left(\frac{\mathrm{Re}_y - \mathrm{Re}_y^*}{A}\right)\right] \text{ and } A = \frac{\left|\Delta \mathrm{Re}_y\right|}{\tanh(0.98)} \tag{6}$$

Boundary conditions for the EWT model replace the standard logarithmic wall law with wall functions proposed by Kader (1981) based on the blending the linear (laminar) and logarithmic (turbulent) wall laws of the form:

$$u^+ = e^{\Gamma} u_{lam}^+ + e^{1/\Gamma} u_{turb}^+ \tag{7}$$

$$\text{where } \Gamma = -\frac{a(y^+)^4}{1+by^+}, \text{ a = 0.01 and b = 5} \tag{8}$$

Further details of the turbulence modelling approach can be found in Fluent (2006).

Numerical method and grid

In the CFD code Fluent, the RANS and turbulence transport equations were discretised using a finite volume method and solved using a point-wise Gauss-Seidel iterative algorithm accelerated by an algebraic Multigrid procedure (Kim et al., 1997; Kim and Rhee, 2002). Second order upwind discretisation was chosen for the convective terms in the transport equations, and the velocity-pressure coupling was resolved via a SIMPLE-type algorithm.

The computational domain consists of three sections. Referring to Fig. 4, Section A (length 1.845 m = 13D) represents the upstream inlet, Section B (length 0.695 m) models the litter trap and overflow channel of the GPT, and section C (length 6.045 m = 10W) accounts for the downstream outflow region. Across the inlet, a uniform mean axial velocity profile corresponding to a measured flow rate of 1.0 L/s was specified. Inlet turbulence levels were specified using values of 0.144 m (turbulence length scale) and 5% (turbulence intensity). Preliminary computations indicated that

varying the upstream turbulence conditions by an order of magnitude had very little influence on the predicted downstream velocity profiles. At the outlet, fully developed uniform flow was assumed by using outflow boundary conditions.

Quadrilateral elements were used to discretise the domain. The internal walls of the trap were modelled as zero thickness and implemented in Fluent as shadow wall boundaries. Two separate grid strategies were employed, depending on the choice of either SKE or EWT turbulence modelling. For the SKE model, nearly uniform grids were used. To investigate the influence of grid refinement on the SKE predictions three grids with mean cell dimensions of 40, 20 and 10 mm (referred to herein as u-gridXX; XX = 40, 20, 10) were created. The coarsest 40 mm grid (u-grid40) is shown in Fig. 4, and the total number of computational cells for the finer 10 mm grid (u-grid10) was 36236. Initial computations using the SKE model on each of these grids yielded near-wall y^+ values to within the acceptable range of $y^+ = 30$ to 500 (Casey and Wintergerste, 2000).

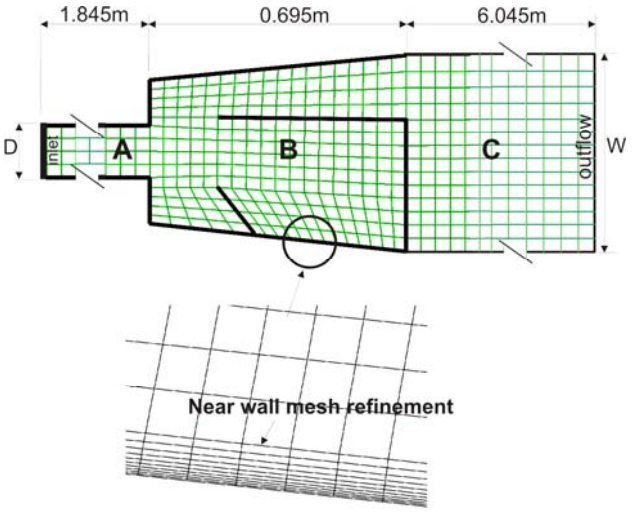

Fig. 4. The computational domain: uniform 40 mm grid, and; detail of near-wall mesh refinement adjoining 6 mm grid.

For the EWT modelling, near-wall mesh refinement was used via the inclusion of 10 transitional layers adjacent to the wetted walls (also shown in Fig. 4). The near-wall grid spacing was successively increased (from 0.2 mm to 1.03 mm) and then joined with a nearly uniformly spaced grid (mean cell width 6 mm, 101432 cells; denoted bl-grid06) inside the bulk of the computational domain. Initial computations on bl-grid06 with the EWT modelling yielded $y^+ < 5$ for the near-wall cell values in the flow domain.

The iterative solver was deemed to have converged and further iterations terminated when a convergence criterion of less than 10^{-5} (c.f. default solver setting of CC = 10^{-3}) for the scaled residuals in the computed mean and turbulence quantities was achieved. In addition, the mass flow rates across the inlet and outlet were also monitored and required to be in agreement to five significant figures. Typically, around 6000 iterations were required for the SKE model, and around 10,000 iterations for the EWT model.

Grid independence

A grid sensitivity study was performed and velocity profiles across the trap mouth for the SKE model computed on ugrid-10, ugrid-20 and ugrid-40 are plotted in Fig. 5. The results on the two finer grids are almost coincident, and consequently ugrid-10 was used. As noted earlier, predictions using EWT modelling were obtained on a grid with maximum spacing of 6 mm (instead of 10 mm) and near-wall mesh refinement, which is also expected to be a

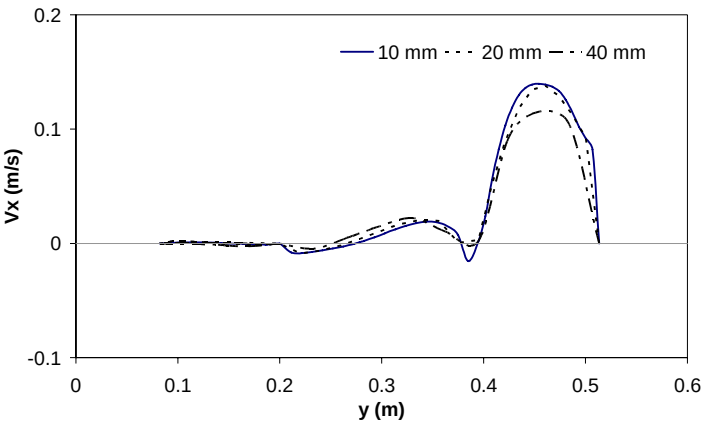

Fig. 5. Axial velocity profiles at station 2.

satisfactory choice based on the above results.

RESULTS AND DISCUSSION

Experimental results

We commence with the discussion of observations of the free surface flow. The main flow structures consist of the deflection of the entry jet into the bypass channel, and the existence of a large inner recirculation flow within the retention area of the trap. Smaller near-wall flow features were also observed. Referring to Fig. 6(a), these are a a top left corner recirculation (L4) and separation zone (L5) in the GPT bypass channel, and three low velocity corner eddies (L7a, L7b & L7c). Although not shown here (see zone 3 in Fig. 8 below), a recirculation zone in front of the baffle was also observed. Such areas may play an important role in litter retention and have been identified as flow structures that can be optimised in GPT design.

Experimental length estimates for the secondary flow structures are tabulated in Fig 6(b). These can be described as dead zones detached or separated from the main stream because of the abrupt geometrical changes, thereby forming their own closed paths behind baffles or obstructions. Dead zones have little net forward flow and are slow to mix or interchange fluid with the main stream, retaining their contents for a longer period of time (Thackston et al., 1987).

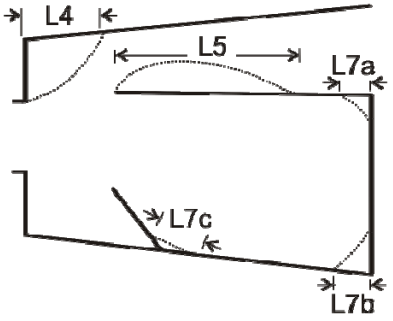

Dim.	Expt	SKE	EWT

(a) (b)

Fig. 6. (a) Key diagram (see Fig 11) (b) experimental and CFD lengths (mm) for the smaller (near wall) flow feature.

The experimentally observed flow structure obtained at a fixed depth of 27 mm from ADV measurements is shown using a vector plot in Fig 7(a). The flow data again shows the strongly deflected jet and the large recirculation zone inside the retention area, as was observed at the free surface. The vector plot also shows a strongly sheared flow across the trap entry which drives the inner recirculation zone. Although near-wall flow data is unable to be measured at this depth due to the limitations of the geometrical configuration of the probe, a dead recirculation zone in front of the baffle can be discerned in the vector plot, similar to the corresponding zone observed at the surface. Qualitatively, the flow structure at this depth is consistent with that observed at the free surface.

Predicted CFD Flow structure

Fig. 7(b) shows the CFD (SKE) predictions for the overall flow in the GPT in form of vector plots. Here, the vector length scales and colour schemes are identical to those used in Fig. 7(a) for ease of comparison with the experimental data. Although direct near-wall comparisons are not possible, away from the boundaries the CFD vector plot is qualitatively similar to the measurements.

The predicted global flow structure at the free surface for both the SKE and EWT models are shown in the form of streamlines in Fig. 8(a) and (b), respectively. Both models predict similar large scale and near-wall flow features, although some differences in the predicted size of these features are evident. In addition to the previously discussed flow features inside the GPT, the predicted streamlines of both models also reveal a diverticulum (zone 2) of the inner recirculation. Re-

examination of the experimental vector plot in Fig. 7(a) also suggests that this flow structure is present at the ADV measurement plane.

In Fig. 6(b), the CFD length predictions for the secondary flow features are compared with the experimental estimates. The tabulated results show that the SKE model predictions are either comparable or too low compared to the experimental results. Furthermore, the EWT model predictions are comparable or higher than the experimental estimates for the near-wall flow features. The comparison suggests that neither CFD model could be considered as clearly superior to the other, despite the significant differences in the near-wall mesh refinement and modelling that are involved.

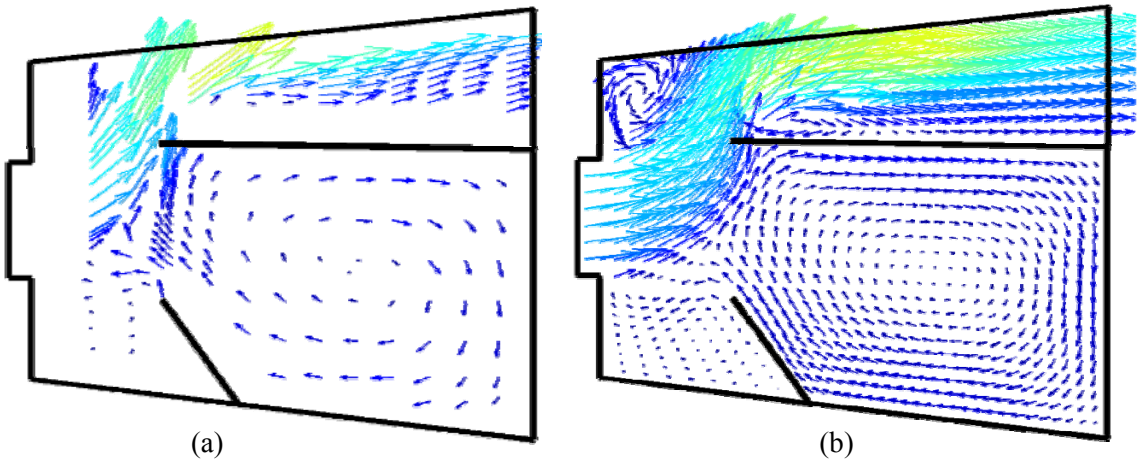

(a) (b)

Fig. 7. Experimental vector plots at 27 mm from the GPT bed for (a) experiment and (b) CFD (SKE).

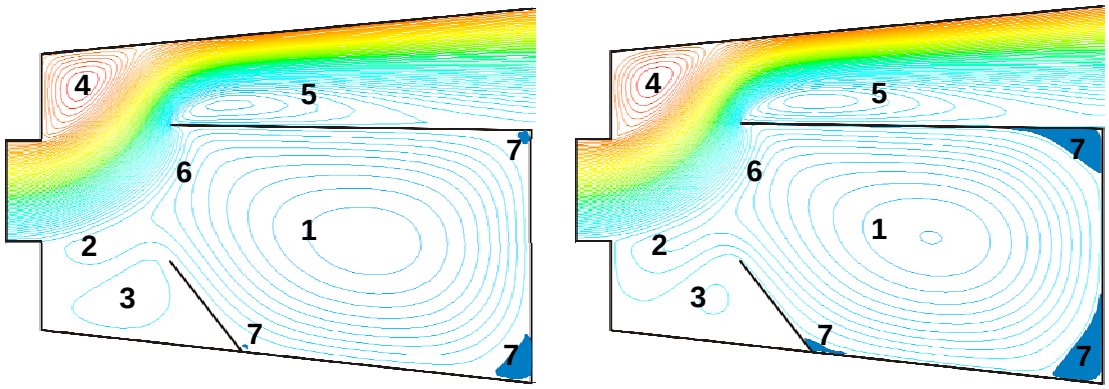

(a) (b)

Feature zones

1, inner recirculation; 2, diverticulum; 3, 4, dead zone (secondary recirculation); 5, flow separation; 6, mixing; 7, low velocity corner eddies.

Fig. 8. Streamlines illustrating global flow structure for (a) SKE (standard two-equation k-ε) or (b) EWT (enhanced wall treatment).

In Fig. 9, a comparison of CFD predictions with experimental results for the axial velocity across Station 1 is shown. Only small differences between the predicted SKE and EWT profiles are noted, and reasonable agreement between computations and experiment can be seen. Axial velocity flow reversal is evident between $0.2 < y < 0.3$ m, consistent with the presence of the diverticulum shown in Fig. 8. However, some discrepancies between the computations and measurements are evident with respect to the extent of the reverse axial flow and the magnitude of the peak height.

Figs. 10 and 11 show further comparisons of the CFD predictions against experimental axial velocity data stations 2 and 3, respectively. The computed profiles are again little different from each other, and both are in fair agreement with experiments. However, it can be seen that the extent of flow reversal in Fig. 10, and the strength of recirculation in Fig. 11, are both under-predicted compared to the experimental data.

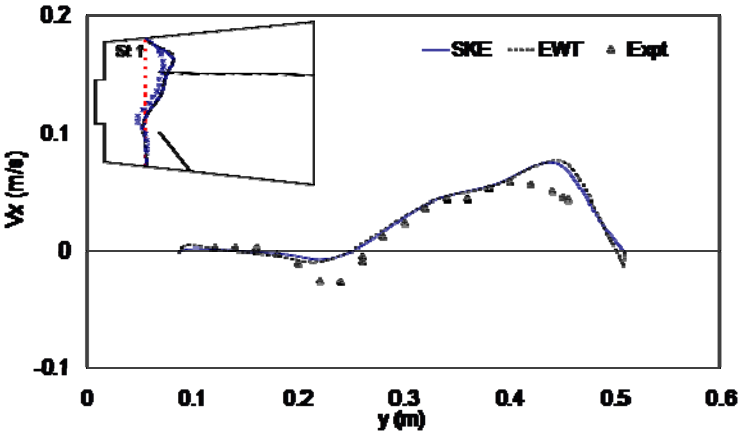

Fig. 9. Axial velocity profiles at station 1, 27 mm from GPT bed, CFD (SKE: standard two-equation k-ε; EWT: enhanced wall treatment) versus experiment (Expt)

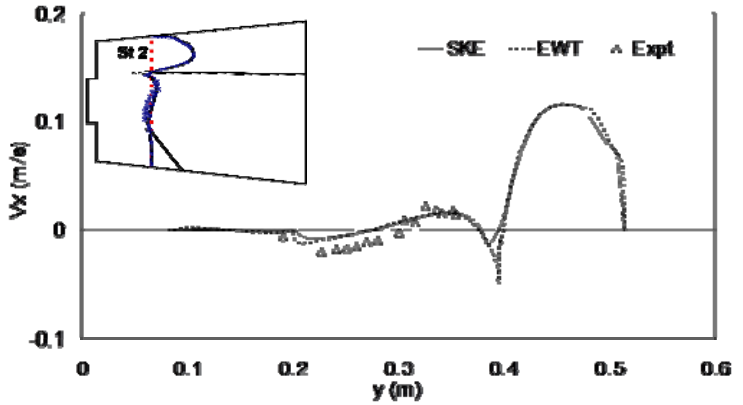

Fig. 10. Axial velocity profiles at station 2, 27 mm from GPT bed, CFD (SKE: standard two-equation k-ε; EWT: enhanced wall treatment;) versus experiment (Expt).

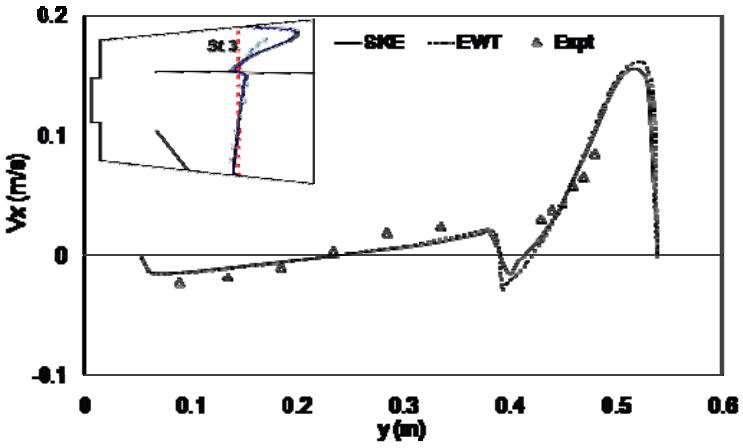

Fig.11. Axial velocity profiles at station 3, 27 mm from GPT bed, CFD (SKE: standard two-equation k-ε; EWT: enhanced wall treatment ;) versus experiment (Expt).

Analysis of near-wall modelling

As noted above, some differences in the SKE and EWT predictions for the near-wall flow features can be seen in the Fig. 6(b) and (8). To understand the source of these differences, the relative influence between the two-layer turbulence modelling and the near wall mesh resolution was investigated.

To this end, a numerical experiment was performed where the SKE model prediction was re-computing on the refined bl-grid06 grid, previously used only for the EWT model. Using this grid, the computed near-wall distance at the first computational cell is $y^+ \approx 1$ for both models and, from equation (8), the boundary condition $U^+ = y^+$ is employed for both the SKE and EWT models. Hence, for this numerical experiment, the wall boundary conditions and bulk flow modelling for both models are the same, and any differences that arise can be attributed to differences in the near wall modelling in the region $1 < Re_y \leq 200$. Figure 12(a) shows the near-wall region where the turbulent Reynolds number (Re_y) is in the range 0–200. Inside this region, the SKE model employs the usual transport equations given in equations (1) and (2), whereas the EWT model employs the one-equation Wolfshtein turbulence model described previously in Section 3.

Figure 12(b) shows a comparison of the predicted mean axial velocities inside the retention area at station 3 using grid bl-grid06 for both the EWT and the SKE models. In the $0 < Re_y \leq 200$ near-wall

region [shaded grey in Fig. 12(b)], the EWT model predicts somewhat greater near-wall peak values than the SKE model. However, these do not result in any major differences between the two profiles across this station in the *unshaded* $Re_y > 200$ bulk flow region illustrated in the figure. A comparison of axial velocity profiles at stations 1 and 2 for the two models (not shown) also shows similar behaviour.

With regard to the size of the dead zones, an examination of streamlines (also not shown for brevity) indicates that SKE predictions on the bl-grid06 have generally increased compared with the lengths tabulated for the SKE model in Fig. 6. For example, L7a = 170 and L5 = 500, and these are now of comparable size to those predicted by the EWT model.

Overall, the above results of this numerical experiment suggest that the use of a refined bl-grid06 mesh with the $U^+ = y^+$ boundary conditions significantly contributes to the change in near-wall flow predictions obtained from the SKE model, while the use of the one-equation Wolfshtein model in the EWT model within the $Re_y \leq 200$ near-wall region contributes a lesser, although noticeable, affect on the peak values.

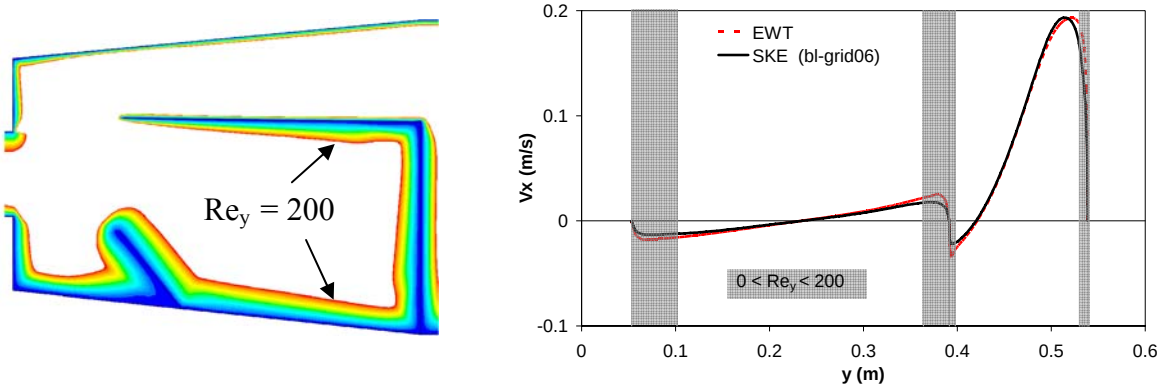

(a) (b)

Fig. 12. (a) near-wall region (Re_y = 0 to 200) and (b) mean axial velocity profiles at station 3 for SKE (standard two-equation k-ε) and EWT (enhanced wall treatment) models computed on bl-grid06 grid.

CONCLUSION

In this study an experimental approach was developed which uses a downstream weir arrangement at the flume outlet to control the nature of the flow and variation in free surface height in a 50% scale model gross pollutant trap (GPT) with fully blocked screens. Fixed depth velocity measurements were taken throughout the trap with an Acoustic Doppler Velocimeter (ADV). Velocity profile data across inlet (station 1), buffer (station 2) and the litter retention (station 3) cross sections of the GPT were taken, suitable for more detailed comparison with simulations. Observations of the near-wall flow features at the free surface were also taken, due to their likely importance for understanding litter capture and retention in the GPT. The experiments showed the existence of main flow structures consisting of a deflected entry jet and a large recirculation zone within the retention area of the GPT. Smaller near-wall flow features were observed and length estimates for these secondary flow structures were made. Qualitatively, the flow structure identified from the fixed depth ADV measurements was consistent with that observed at the free surface.

Complementary CFD modelling (using Fluent 6.3) was performed using a two-dimensional k-ε turbulence model along with either standard wall law boundary conditions or enhanced near-wall

modelling approaches. Both models predicted surface flow structures which were consistent with those observed experimentally. However, the results suggest that neither CFD modelling approach could be considered as clearly superior to the other, despite the significant differences in the near-wall mesh refinement and modelling that are involved. Numerical experiments suggest that much of the differences in predictions obtained using standard and enhanced wall modelling can be accounted for by the use of greater near-wall grid refinement, while the use of enhanced near-wall modelling in the $0 < Re_y \leq 200$ region has a lesser, but still noticeable, affect.

The experimental approach taken here was found useful to control the flow regime in the GPT and further experiments are recommended to study a greater range of flow conditions.

Acknowledgements
The authors acknowledge C-M Concrete Pty. Ltd, 2004 (Mr Phil Thomas) for their ARC linkage grant support and David Graham and Michael Roomina for their technical support in using Fluent. We also thank the QUT workshop portfolio and the QUT High Performance Computing & Research Support staff for their support with the facilities and services used in this study.

References
Allison, R. A., Chiew, F. H. S. and McMahon, T. A. (1998). *From roads to rivers: gross pollutant removal from urban waterways*. In: Report 98/6, Co-operative Research Centre for Catchment Hydrology (eWater CRC), University of Canberra, Australia.
http://www.catchment.crc.org.au/pdfs/technical199806pt1.pdf (accessed 22 February 2008).
Armitage, N. P. and Rooseboom, A. (1999). The removal of litter from stormwater conduits in the developing world. *Water Science and Technology*, 39(9), 277–284.
Buxton, A., Tait, S., Stovin, V., and Saul, A. (2002). Developments in a methodology for the design of engineered invert traps in combined sewer systems. *Water Science and Technology*, 45(7), 133–142.
Casey, M. and Wintergerste, T. (Eds) (2000). *ERCOFTAC Special Interest Group on Quality and Trust in Industrial CFD: Best Practices Guidelines*. Version 1.0, European Research Community on Flow Turbulence and Combustion (ERCOFTAC).
Cea, L., Puertas, J., & Vázquez-Cendón, M. E. (2007). Depth Averaged Modelling of Turbulent Shallow Water Flow with Wet-Dry Fronts. Archives of Computational Methods in Engineering, 14(3), 303-341.
Faram, M. G. and Harwood, R. (2003). A method of the numerical assessment of sediment interceptors. *Water Science and Technology* 47(4), 167–174.
Fluent (2006). *Fluent 6.3 User's Guide*. Fluent, Inc, Lebanon, USA.
Gupta, K., Mehta; P., Thinglas, T., Tait , S. J. and Stovin, V. (2005). Optimization of sediment trap configuration using CFD modelling for Indian drainage systems. In: *10th International Conference on Urban Drainage (10ICUD)*, August 21–26, Copenhagen, Denmark.
Harwood R., (2002). CSO modelling strategies using computational fluid dynamics. In: *Proceedings of the 9th International Conference on Urban Drainage (9ICUD)*, Global Solutions for Urban Drainage, Portland, USA.
Huggins, D. L., Piedrahita, R. H. and Rumsey, T. (2004) Analysis of sediment transport modelling using computational fluid dynamics (CFD) for aquaculture raceways. *Aquacultural Engineering*, 31(3–4), 277–293.
Jongen, T. (1992) *Simulation and modeling of turbulent incompressible flows*, Ph.D. Thesis, EPF Lausanne, Lausanne, Switzerland.
Kader, B. A. (1981). Temperature and concentration profiles in fully turbulent boundary layers. International Journal of Heat and Mass Transfer, 24(9), 1541-1544.

Kim, S-E. and Rhee, S. H. (2002). *Assessment of eight turbulence models for a three-dimensional boundary layer involving crossflow and streamwise vortices*. Technical report, TN165, Fluent Inc., Lebanon, USA.
Kim, S-E., Mathur, S. R., Murthy, J. Y. and Choudhury, D. (1997). *A Reynolds-Averaged Navier Stokes Sovler using an unstructured mesh based finite-volume scheme*. Technical report, TN117, Fluent Inc., Lebanon, USA.
Kraus, N. C., Lohrmann A. and Cabrera R. (1994). New acoustic meter for measuring 3D laboratory flows. *Journal of Hydraulic Engineering*, 120, 406–412.
Kwon S. B., Park, N. S., Lee, S. J., Ahn, H. W. and Wang, C. K. (2006). Examining the effect of length/width ratio on the hydro-dynamic behaviour in a DAF system using CFD and ADV techniques. *Water Science & Technology*, 53(7), 141–149.
Lohrmann A, Cabrera R, Kraus NC. (1994). Acoustic-Doppler velocimeter (ADV) for laboratory use. In: *Proceeding of Conference on Fundamentals and Advancements in Hydraulic Measurements and Experimentation*, (Ed. C. A. Pugh.) pp. 351–365, American Society of Civil Engineers, Buffalo, New York.
Lundh, M., Jonsson, L. and Dahlquist, J. (2001). The flow structure in the separation zone of a DAF pilot plant and the relation with bubble concentration. *Water Science and Technology,* 43(8), 185–194.
McLelland, S. J., and Nicholas, A. P. (2000). A new method for evaluating errors in high-frequency ADV measurements. *Hydrological Processes*, 14, 351–366.
Park, N., Lim, J., Lee, S., Lee, K. and Kwon, S. (2006). Examining the effect of transverse troughs on hydrodynamic behaviour in a sedimentation basin with CFD simulation and ADV technique. *Journal of Water: Research and Technology – Aqua,* 55(4), 247–256.
Phillips, D. I. (1999). A new litter trap for urban drainage systems. *Water Science and Technology* Vol. 39(2), 85–92.
Rastogi, A. K. W., Rodi, 1978, Predictions of heat and mass transfer in open channels. *Journal of Hydraulic Engineering*, ASCE, 104(3), 397-420.
SonTek/ YSI , 2006. ADVField/ Hydra Acoustic Doppler Velocimeter (Field) Technical Documentation. CDROM: P/ N 6055-00005 rev – E. 6837. Nancy Ridge Drive, San Diego, CA 92121, USA.
Stovin, V. R., and Saul A. J. (2000). Computational fluid dynamics and the design of sewage storage chambers. *Water and Environmental Management,* 14(2), 103–110.
Stovin, V. R., Saul, A. J., Drinkwater, A. and Clifforde, I. (1999). Field testing CFD-based predictions of storage chamber gross solid separation efficiency. *Water Science and Technology*, 39(9), 161–168.
Stovin, V. R., Grimm, J. P., Buxton, A. P. and Tait, S. J. (2002). Parametric Studies on CFD studies Models of Sewage Structures. In: *Proceedings of the 9th International Conference on Urban Drainage (9ICUD)*, Global Solutions for Urban Drainage, Portland, USA.
Ta, C. T., Beckley, J. and Eades, A. (2001). A multiphase CFD model of a DAF Process. *Water Science and Technology*, 43(8), 153–157.
Thackston, E. L., Shields, D. F. and Schroeder P. R. (1987). Residence time distributions of shallow basins. *Journal of Environmental Engineering*, 113(6), 1319–1332.
Tyack, J. N. and Fenner, R. A. (1999). Computational fluid dynamics modelling of velocity profiles within a hydrodynamic separator. *Water Science and Technology*, 1999. 39(9): p. 169-176.
Voulgaris G. and Trowbridge J. H. (1998). Evaluation of the Acoustic Doppler Velocimeter (ADV) for turbulence measurements. *Journal of Atmospheric and Oceanic Technology,* 15, 272–289.
Wahl, T. L. (2006). A window-based viewing and post-processing utility for Acoustic Doppler Velocimeter (ADV) data files. http://www.usbr.gov/pmts/hydraulics_lab/twahl/winadv/ (accessed 12 December 2006).

Wolfshtein, M., (1969). The velocity and temperature distribution of one-dimensional flow with turbulence augmentation and pressure gradient. *International Journal of Heat Mass Transfer*, 12, 301–318.